THE JOURNAL OF PHYSICAL CHEMISTRY LETTERS
A JOURNAL OF THE AMERICAN CHEMICAL SOCIETY

pubs.acs.org/JPCL Letter

Observation of the Transition from Triple Bonds to Single Bonds between Ru−Ge Bonding in $RuGeO(CO)_n^-$ (n = 3−5)

Ziheng Zhang, Zicheng Ling, Bangmin Ju, Gang Li, Qinqin Yuan,* Longjiu Cheng,* Hua Xie,* and Ling Jiang

Cite This: J. Phys. Chem. Lett. 2024, 15, 6952−6957 Read Online

ACCESS | Metrics & More | Article Recommendations | Supporting Information

ABSTRACT: This work reports the observation and characterization of heterobinuclear transition-metal main-group metal oxide carbonyl complex anions, $RuGeO(CO)_n^-$ (n = 3−5), by combining mass-selected photoelectron velocity map imaging spectroscopy and quantum chemistry calculations. The experimentally determined vertical electron detachment energy of $RuGeO(CO)_3^-$ surpasses those of $RuGeO(CO)_4^-$ and $RuGeO(CO)_5^-$, which is attributed to distinctive bonding features. $RuGeO(CO)_3^-$ manifests one covalent σ and two Ru-to-Ge dative π bonds, contrasting with the sole covalent σ bond present in $RuGeO(CO)_4^-$ and $RuGeO(CO)_5^-$. Unpaired spin density distribution analysis reveals a 17-electron configuration at the Ru center in $RuGeO(CO)_3^-$ and an 18-electron configuration in $RuGeO(CO)_4^-$ and $RuGeO(CO)_5^-$. This work closes a gap in the quantitative physicochemical characterization of heteronuclear oxide carbonyl complexes, enhancing our insights into catalytic processes of CO/GeO on the metal surface at the molecular level.

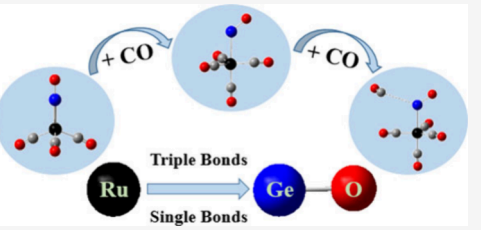

Carbon monoxide (CO) oxidation on bulk material surfaces is pivotal in numerous industrial processes, such as Fischer−Tropsch chemistry, acetic acid synthesis, alcohol synthesis, and hydroformylation.[1−5] Metal clusters representing low-coordinate sites on surfaces are often used as models for studying the surface chemistry of bulk materials, which can provide valuable insights into the alteration of chemical bonds on the most active or least coordinated sites of a catalyst.[6−10] Moreover, the synergy effects observed in the chemical processes are expected to be responsible for the high catalytic performance of heterobinuclear metal complexes.[11−13] Therefore, investigating heterobinuclear metal and metal oxide carbonyls represents an ideal model system,[14−18] because such studies not only yield significant understanding of the chemical bonding nature of metal−metal or metal−carbon interactions at the molecular level but also aid in comprehending the synergy effects of various transition metals on the catalytic performance of CO absorption on metal surfaces.

Recently, gaseous heterobinuclear metal−iron carbonyls have been generated and characterized utilizing mass-selected infrared spectroscopy and photoelectron spectroscopy, combined with advanced quantum chemistry calculations.[19−32] For all heterobinuclear metal−iron carbonyls, the CO ligands were found to adopt a common terminal coordination to the metal atoms. However, diverse chemical bonding features, including covalent metal−metal single or multiple bonds, were identified for the metal−iron interactions depending on the CO ligand numbers and the electropositive nature of the metals,[29,31] such as a half bond in $ZnFe(CO)_5^+$ carbonyl,[30] a σ single bond in the $MgFe(CO)_4^-$ structure,[23] one σ single bond and two dative π bonds in $BeFe(CO)_4$ and $UFe(CO)_3^-$,[24,25] a triple bond in $AFe(CO)_3$ (A = Ge, Sn, Pb, As, Sb, and Bi),[26,27] and an unprecedented quadruple-bond interaction for $AFe(CO)_3$ (A = Sc, Y, La).[28] Heterodinuclear iron oxide carbonyls, represented by $OUFe(CO)_3^-$, exhibit an identical chemical bonding profile to $UFe(CO)_3^-$.[25] So far, heterodinuclear metal oxide carbonyls simultaneously containing both main group and transition metals remain unexplored. Given the significant role of heterobinuclear oxide carbonyls in CO oxidation via the Langmuir−Hinshelwood-like mechanism, further research in this field is warranted.

Main group metal element germanium (Ge) and its oxides have important applications in fields like aerospace, solar cells, and biomedicine, in addition to their potential as catalysts in the optical industry.[33−37] Moreover, ruthenium (Ru), as a homotope of iron, has similar chemical reactivity.[38−40] Investigating the reaction of CO with the Ru−GeO heterodimers would not only help understand the chemical bonding between main group metal and transition metal but also can be used as a model system to study CO/GeO oxidation on metal surface from the molecular level, thereby facilitating the exploration and development of novel catalysts.

For this purpose, we performed laser vaporization of Ge−Ru alloy rods in a buffer gas atmosphere comprising 5% CO

Received: May 24, 2024
Revised: June 24, 2024
Accepted: June 27, 2024
Published: June 28, 2024

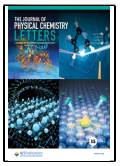

https://doi.org/10.1021/acs.jpclett.4c01532
J. Phys. Chem. Lett. 2024, 15, 6952−6957

seeded in helium to yield a series of heterobinuclear transition metal−main group metal oxide carbonyls, among which the $RuGeO(CO)_n^-$ (n = 3−5) cluster anions that we are interested in are mass-selected and characterized by photoelectron velocity map imaging spectroscopy with 355 nm photons. The detailed experimental process is listed in the Supporting Information. The recorded 355 nm photoelectron spectra (PES) of $RuGeO(CO)_n^-$ (n = 3−5) are exhibited in Figure 1,

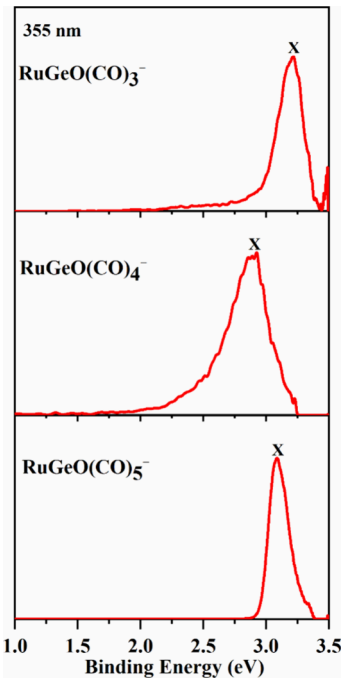

Figure 1. Photoelectron spectra of $RuGeO(CO)_n^-$ (n = 3−5) at 355 nm (3.496 eV).

all exhibiting a single broad band labeled as X without any discernible vibrational details being resolved. The experimental vertical detachment energy (VDE) values, directly measured from the band maximum of each spectrum, do not follow a monotonically increasing trend with the number of CO ligands but, rather, showcase where $RuGeO(CO)_3^-$ (3.20 eV) > $RuGeO(CO)_4^-$ (2.89 eV) < $RuGeO(CO)_5^-$ (3.08 eV). However, according to the previously reported PES results of $M(CO)_n^-$,[13] the negatively charged electron is commonly stabilized upon the progressive binding of CO molecules, which renders an increase in VDEs with cluster size. Thus, the nonmonotonic behavior observed in the VDE values may imply significant transitions of geometrical and electronic structures upon electron detachment. In addition, the hot bands substantially contribute to the broad bands for the n = 3 and 4 complexes, characterized by exceptionally prolonged and gentle rising edges. A close examination indicates that $RuGeO(CO)_4^-$ has a larger slower front rising edge than that in n = 3, which is attributed to the hot band and a possible two-photon process due to the different bonding properties between them (see subsequent structral discussion), as in previously reported $[B_2(CN)_6]^{2-}$ dianion.[41] Consequently, determining the adiabatic detachment energy (ADE) value directly from the spectral onset is unfeasible; instead, it is derived by extending a line from the leading edge of the VDE peak and adding the instrumental resolution at the point where the line intersects with the horizontal axis. As a result, the ADE values of $RuGeO(CO)_n^-$ (n = 3−5) are estimated to be 2.65 ± 0.04 eV, 2.20 ± 0.06 eV, and 2.93 ± 0.03 eV, respectively, demonstrating a comparable trend to the VDE values.

On the basis of the experimentally recorded photoelectron spectra, quantum chemical calculations were performed to locate the encoded geometric and electronic structures and aid in spectral assignments (refer to the Supporting Information for details). For each $RuGeO(CO)_n^-$ (n = 3−5), nine low-lying isomers labeled as *n*a-*n*i, along with their relative energies (REs), were calculated and are provided in Figures S1−S3. Following the Boltzmann distribution law, only the three lowest-energy isomers for each complex anion, as depicted in Figure 2, were considered for further ADE/VDE value

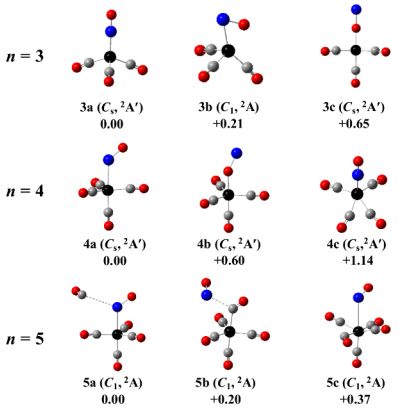

Figure 2. Optimized structures of the lowest-energy isomers for $RuGeO(CO)_n^-$ (n = 3−5) (Ge, blue; Ru, black; C, gray; O, red). Relative energies are given in eV.

calculations and spectral simulations to identify the structures that contribute to experiments. Table 1 compares the calculated REs, ADE, and VDE values of these isomers at the B3LYP/6-311G(d) (Ge, C, and O)/def2-TZVPP (Ru) level. Apparently, the high-lying **3b**, **3c**, **4b**, **4c**, **5b**, and **5c** isomers can be readily ruled out due to their relatively high REs of at least 0.20 eV, considerably smaller ADE/VDE values, and distinctively different simulated spectral patterns relative to the experimental results (Figure S4). In contrast, the calculated ADE/VDE values of 2.45/3.23, 2.06/2.99, and 2.82/2.98 eV for the lowest-lying **3a**, **4a**, and **5a** isomers are in excellent agreement with the corresponding experimental data of 2.65/3.20, 2.20/2.89, and 2.93/3.08 eV (Table 1), respectively. The simulated density of states (DOS) spectra[42] in Figure S4 also nicely reproduce the experimental spectral contours, further confirming the exclusive existence of these lowest-lying isomers.

The **3a** isomer possesses a $^2A'$ electronic state with C_s symmetry, where all three carbonyl ligands coordinate to the Ru center, and the GeO group is also bonded to the Ru atom via the less electronegative Ge atom, forming a triangular pyramid geometry. Similar to the previously reported heterobinuclear metal−iron clusters $MFe(CO)_4^-$ (M = Be, Mg, Ti, V, and Cr),[16,23,24] the **4a** isomer shares the same geometric symmetry and electronic state as **3a**, featuring three terminal CO ligands in the equatorial plane, one terminal CO ligand in the axial plane, and a terminal GeO ligand with an obtuse Ru−Ge−O angle. In the **5a** isomer, the building block of **4a** remains largely unchanged, while the fifth CO loosely interacts with the Ge atom via physical absorption. The bond

https://doi.org/10.1021/acs.jpclett.4c01532
J. Phys. Chem. Lett. 2024, 15, 6952−6957

Table 1. Comparison of Experimental VDE and ADE Values (in eV) to B3LYP/6-311G(d) (Ge, C, O)/def2-TZVPP (Ru) Calculated Results of the Lowest-Energy Isomers for $RuGeO(CO)_n^-$ (n = 3−5)

			VDE		ADE	
Cluster	Isomer	Relative energy (eV)	Expt.[z]	Calc.	Expt.[z]	Calc.
$RuGeO(CO)_3^-$	**3a**	0.00	3.20(1)	3.23	2.65(4)	2.45
	3b	0.21		2.37		1.80
	3c	0.65		1.84		1.67
$RuGeO(CO)_4^-$	**4a**	0.00	2.89(3)	2.99	2.20(6)	2.06
	4b	0.60		1.88		1.57
	4c	1.14		2.69		2.10
$RuGeO(CO)_5^-$	**5a**	0.00	3.08(2)	2.98	2.93(3)	2.82
	5b	0.20		2.69		2.58
	5c	0.37		2.46		2.26

[z]Numbers in parentheses represent the uncertainty in the last digit.

lengths and Wiberg bond indices (WBIs) orders of the Ge−Ru bonds in $RuGeO(CO)_n^-$ (n = 3−5) anions are detailed in Table 2. Notably, the Ge−Ru distance in $RuGeO(CO)_3^-$ (2.350 Å) is much shorter than that in $RuGeO(CO)_4^-$ (2.642 Å) and $RuGeO(CO)_5^-$ (2.632 Å), consistent with the calculated WBIs of 1.084 (**3a**), 0.584 (**4a**), and 0.592 (**5a**). The variation of bond distances and orders, as well as the decreasing Ru−Ge−O angle from **3a** to **4a** and **5a**, suggests a change in the Ru−Ge bonding nature. The C−O/Ge−O bond distances in all complexes were calculated to be around 1.16/1.65 and 1.67 Å (Figure S5), slightly longer than those of free CO/GeO molecules (1.13/1.63 Å), suggesting weakening of the C−O/Ge−O bonds.

Table 2. Ge−Ru Bond Lengths (Å), Bond Orders of $RuGeO(CO)_n^-$ (n = 3−5) Calculated at the B3LYP/6-311G(d) (Ge, C, O)/def2-TZVPP (Ru) Level of Theory

Species	Ge−Ru bond length	Wiberg bond order
$RuGeO(CO)_3^-$	2.35	1.08
$RuGeO(CO)_4^-$	2.64	0.58
$RuGeO(CO)_5^-$	2.63	0.59

To further elucidate the chemical bonding properties of the Ru−Ge interaction in the lowest-lying n**a** structures of $RuGeO(CO)_n^-$ (n = 3−5), an analysis of their frontier molecular orbitals was conducted. Figure 3 illustrates the highest occupied molecular orbitals (HOMO) extending to the sixth valence molecular orbital from the HOMO, with relative orbital energies provided. The orbital composition analyses using the natural atomic orbital (NAO) method of the frontier Kohn-Shan MOs for these species are shown in Tables S3−S5. For $RuGeO(CO)_3^-$, the HOMO and HOMO−1 are featured by two dative π-type Ru-to-Ge interactions, with an orbital composition contribution of 64% (hybrid orbitals of Ru: 29% 4d + 1% 5s + 27% 5p; Ge 7% 4p) and 64% (hybrid orbitals Ru: 43% 4d + 17% 5p; Ge: 4% 4p), respectively. The HOMO−2 (−2.18 eV), an energy degenerate orbital of HOMO−1 (2.15 eV), is an evident σ-type Ru−Ge electron-sharing bonding orbital formed from the combination of Ru 4d and 5p hybrid orbitals (39% 4d + 14% 5p) and Ge 4s and 4p hybrid orbitals (10% 4s + 2% 4p). The HOMO−3 and HOMO−4 predominantly consist of 70% contributions from the 3d orbitals of the Ru atom, showcasing notable Ru 3d to CO 2p* back-donation. HOMO−5 and HOMO−6 refer to Ge−O π bonding orbitals exhibiting characteristics analogous to the C−O bonding. The analysis of HOMO, HOMO−1, and HOMO−2 reveals that the Ru−Ge bonding in $RuGeO(CO)_3^-$ involves one electron-sharing σ bonding as well as two additional dative π bonding interactions, reminiscent of the recently reported metal−metal triple bonding in $AFe(CO)_3^-$ (A = Ge, Sn, Pb, As, Sb, and Bi), $UFe(CO)_4^-$, and $OUFe(CO)_3^-$ complexes.[25−27]

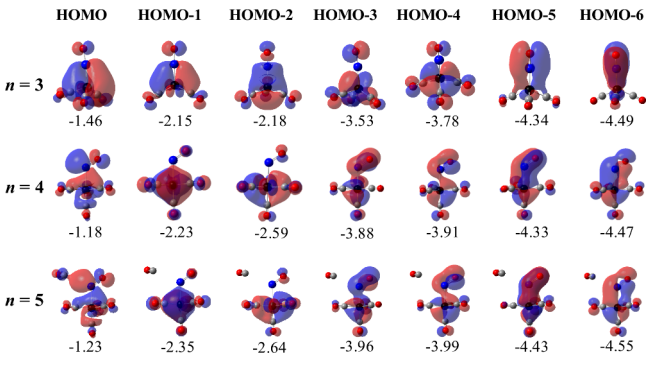

Figure 3. Molecular orbitals of the most stable isomers for $RuGeO(CO)_n^-$ (n = 3−5) calculated at the B3LYP/6-311G(d) (Ge, C, O)/def2-TZVPP (Ru) level of theory, showing the highest occupied molecular orbitals (HOMOs) down to the sixth valence molecular orbital from the HOMO. Energies are given in eV.

In the cases of $RuGeO(CO)_4^-$ and $RuGeO(CO)_5^-$, the HOMO is dominated by a σ-type Ru−Ge electron-sharing bonding orbital with composition of 63% (hybrid orbitals Ru: 15% 4d + 10% 5p; hybrid orbitals Ge: 13% 4s + 25% 4p) and 60% (hybrid orbitals Ru: 15% 4d + 9% 5p; hybrid orbitals Ge: 12% 4s + 24% 4p), respectively. The HOMO−2 and HOMO−3 demonstrate significant Ru 3d to CO 2p* back-donation, while the remaining orbitals are too complex for further assignment. No similar dative π-bonding interactions are discovered between the Ru and Ge atoms. Additionaly, a distinct interaction between the fifth CO and Ge is evident from the HOMO of $RuGeO(CO)_5^-$. Based on their chemical bonding characteristics, $RuGeO(CO)_4^-$ and $RuGeO(CO)_5^-$ can be analogously viewed as monometal carbonyl complexes akin to the recently reported $Fe(CO)_5^-$ and $Fe(CO)_6^-$ complex anions.[31] This implies that the oxides of Ge and C in the same main group, namely, GeO and CO, present a similar chemical bonding property within these metal carbonyl complexes, thereby demostrating the semimetal nature of Ge.

To gain more chemically intuitive pictures of the different bonding modes within $RuGeO(CO)_3^-$ and $RuGeO(CO)_4^-$, adaptive natural density partitioning (AdNDP) analysis was

https://doi.org/10.1021/acs.jpclett.4c01532
J. Phys. Chem. Lett. 2024, 15, 6952−6957

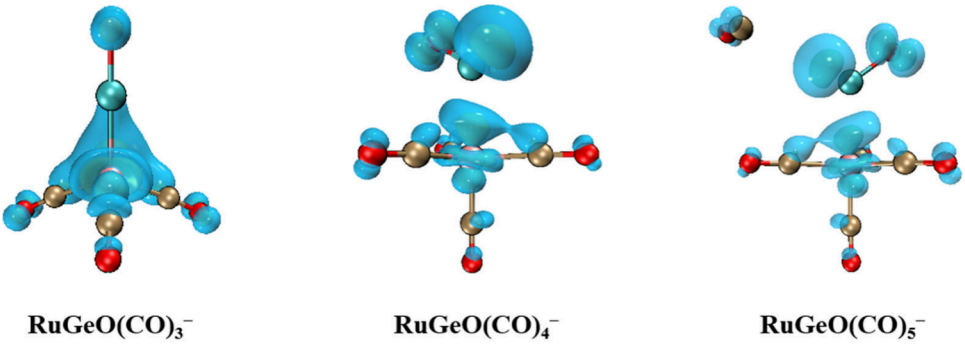

Figure 4. Isosurface map of unpaired spin density distributions for the most stable isomers of $RuGeO(CO)_n^-$ (n = 3−5) calculated at the B3LYP/6-311G(d) (Ge, C, O)/def2-TZVPP (Ru) level of theory (Isosurface value = 0.003).

conducted and shown in Figure S7. Given that $RuGeO(CO)_n^-$ complexes are all open-shell species, only the α electrons are selectively analyzed, which also reveals one covalent σ and two Ru-to-Ge dative π bonds within $RuGeO(CO)_3^-$, contrasting with the sole covalent Ru−Ge σ bond found in $RuGeO(CO)_4^-$.

The disparity in chemical bonding partially elucidates why the experimental VDE value of $RuGeO(CO)_3^-$ (3.20 eV) exceeds those of $RuGeO(CO)_4^-$ (2.89 eV) and $RuGeO(CO)_5^-$ (3.08 eV). The evolution of the HOMO energy also parallels the changing trend in ADE/VDE values. To pinpoint the electron detachment site more precisely, isosurface map illustrating unpaired spin density distributions for $RuGeO(CO)_n^-$ (n = 3−5) are computed and visualized in Figure 4, revealing that the majority of spin densities are located on the center Ru atom for $RuGeO(CO)_3^-$, while they are concentrated on the antiorbital of Ge−O for $RuGeO(CO)_4^-$ and $RuGeO(CO)_5^-$. Accordingly, the Ru center adopts a 17-electron configuration in $RuGeO(CO)_3^-$ and an 18-electron configuration in the other two complexes. Obviously, electron detachment from the antiorbital is more favorable, thereby partially accounting for the observed decreasing followed by increasing VDE trend across the $RuGeO(CO)_n^-$ (n = 3−5) series.

What is on earth responsible for the alteration of the bonding characteristics with the gradual augmentation of the CO ligands? The weaker electronegativity of the Ge atom compared to that of the C atom leads to diminished repulsion between Ge and Ru in contrast to C and Ru, as evidenced by the electrostatic potential energy in Figure S6. On the other hand, the Ge≡O bonding withdraws electron density from Ge to the O atom, facilitating electron migration from Ru orbitals into the Ge≡O antibonding orbital. This mechanism mirrors the stronger and shorter U≡Fe bond in the case of $OUFe(CO)_3^-$ relative to that of $UFe(CO)_3^-$. Furthermore, the Ru−Ge interaction is attenuated by the trans effect arising from the axial coordination of the CO to Ru in $Ru(CO)_4$ for $RuGeO(CO)_4^-$ and $RuGeO(CO)_5^-$.

In this study, a series of heterobinuclear transition-metal-main-group metal oxide carbonyls, $RuGeO(CO)_n^-$ (n = 3−5), generated via a laser vaporization supersonic cluster source, are characterized by combining mass-selected photoelectron velocity map imaging spectroscopy and theoretical calculations. The experimentally observed nonmonotonic ADE/VDE value trend indicates a significant transition in both the geometrical and electronic structures that contributes to experiments. Chemical bonding analysis reveals that $RuGeO(CO)_3^-$ exhibits all carbonyl ligands bound to the Ru center, featuring Ru−Ge multiple bonds involving one covalent σ and two Ru-to-Ge dative π bonds. In $RuGeO(CO)_4^-$, three terminal CO ligands are positioned in the equatorial plane, along with one terminal CO ligand in the axial plane and a terminal GeO ligand forming a Ru−Ge σ bond. In $RuGeO(CO)_5^-$, the fifth CO loosely interacts to Ge atom through physical absorption, building upon the structure of $RuGeO(CO)_4^-$. This work closes a gap in the quantitative physicochemical characterization of heteronuclear oxide carbonyl complexes and provides a better understanding of the catalytic reaction of CO and GeO on transition-metal surfaces at the molecular level.

■ ASSOCIATED CONTENT

Supporting Information

The Supporting Information is available free of charge at https://pubs.acs.org/doi/10.1021/acs.jpclett.4c01532.

Experimental methods and computational details; Optimized structures of the low-energy isomers for $RuGeO(CO)_n^-$ (n = 3−5) cluster anions at the B3LYP/6-311G(d) (Ge, C, O)/def2-TZVPP (Ru) level of theory(Figures S1−S3); comparison of experimental 355 nm photoelectron spectra (bottom rows) of $RuGeO(CO)_n^-$ (n = 3−5) to the simulated spectra of the three lowest-energy isomers (top rows) (Figure S4); optimized structures with key bond lengths (Å) noted for the $RuGeO(CO)_n^-$ (n = 3−5) complexes (Figure S5); electrostatic potential surface of CO and GeO (Figure S6); adaptive natural density partitioning (AdNDP) bonding patterns based on the α electrons of (a) $RuGeO(CO)_3^-$ and (b) $RuGeO(CO)_4^-$, respectively (Figure S7); comparison of experimental VDE value of $RuGeO(CO)_3^-$ to the calculated ones for the most stable structure (Table S1); contributions of the relative energies (eV) for different spin multiplicities in the $RuGeO(CO)_n^-$ (n = 3−5) species (Table S2); orbital composition analysis (in %) by natural atomic orbital (NAO) method to the frontier KS-MOs of the most stable isomer for $RuGeO(CO)_n^-$ (n = 3−5) cluster anions (Table S3−S5) (PDF)

Transparent Peer Review report available (PDF)

■ AUTHOR INFORMATION

Corresponding Authors

Qinqin Yuan − *Department of Chemistry, Key Laboratory of Functional Inorganic Materials of Anhui Province, Anhui*

https://doi.org/10.1021/acs.jpclett.4c01532
J. Phys. Chem. Lett. 2024, 15, 6952−6957

University, Hefei 230601, China; orcid.org/0000-0001-5771-6147; Email: qinqinyuan@ahu.edu.cn

Longjiu Cheng − *Department of Chemistry, Key Laboratory of Functional Inorganic Materials of Anhui Province, Anhui University, Hefei 230601, China;* orcid.org/0000-0001-7086-6190; Email: clj@ustc.edu

Hua Xie − *State Key Laboratory of Molecular Reaction Dynamics, Dalian Institute of Chemical Physics, Chinese Academy of Sciences, Dalian 116023, China;* orcid.org/0000-0003-2091-6457; Email: xiehua@dicp.ac.cn

Authors

Ziheng Zhang − *Department of Chemistry, Key Laboratory of Functional Inorganic Materials of Anhui Province, Anhui University, Hefei 230601, China; State Key Laboratory of Molecular Reaction Dynamics, Dalian Institute of Chemical Physics, Chinese Academy of Sciences, Dalian 116023, China*

Zicheng Ling − *Department of Chemistry, Key Laboratory of Functional Inorganic Materials of Anhui Province, Anhui University, Hefei 230601, China*

Bangmin Ju − *State Key Laboratory of Molecular Reaction Dynamics, Dalian Institute of Chemical Physics, Chinese Academy of Sciences, Dalian 116023, China*

Gang Li − *State Key Laboratory of Molecular Reaction Dynamics, Dalian Institute of Chemical Physics, Chinese Academy of Sciences, Dalian 116023, China;* orcid.org/0000-0001-5984-111X

Ling Jiang − *State Key Laboratory of Molecular Reaction Dynamics, Dalian Institute of Chemical Physics, Chinese Academy of Sciences, Dalian 116023, China;* orcid.org/0000-0002-8485-8893

Complete contact information is available at: https://pubs.acs.org/10.1021/acs.jpclett.4c01532

Notes

The authors declare no competing financial interest.

■ ACKNOWLEDGMENTS

The authors gratefully acknowledge the Dalian Coherent Light Source (DCLS) for support and assistance. This work was supported by the National Natural Science Foundation of China (Grant Nos. 22273001, 22273101, 22125303, 92061203, and 22288201), the Scientific Instrument Developing Project of the Chinese Academy of Sciences (GJJSTD20220001), the International Partnership Program of the Chinese Academy of Sciences (121421KYSB20170012), and Dalian Institute of Chemical Physics (DICP I202437).

■ REFERENCES

(1) Freund, H.-J.; Meijer, G.; Scheffler, M.; Schlögl, R.; Wolf, M. CO Oxidation as a Prototypical Reaction for Heterogeneous Processes. *Angew. Chem., Int. Ed.* **2011**, *50* (43), 10064−10094.

(2) Luo, Z. X.; Castleman, A. W., Jr.; Khanna, S. N. Reactivity of Metal Clusters. *Chem. Rev.* **2016**, *116* (23), 14456−14492.

(3) Zhou, M. F.; Andrews, L.; Bauschlicher, C. W. Spectroscopic and Theoretical Investigations of Vibrational Frequencies in Binary Unsaturated Transition-Metal Carbonyl Cations, Neutrals, and Anions. *Chem. Rev.* **2001**, *101* (7), 1931−1962.

(4) Xu, Q. Metal Carbonyl Cations: Generation, Characterization and Catalytic Application. *Coord. Chem. Rev.* **2002**, *231* (1), 83−108.

(5) Ricks, A. M.; Reed, Z. E.; Duncan, M. A. Infrared Spectroscopy of Mass-Selected Metal Carbonyl Cations. *J. Mol. Spectrosc.* **2011**, *266*, 63−74.

(6) Böhme, D. K.; Schwarz, H. Gas-Phase Catalysis by Atomic and Cluster Metal Ions: The Ultimate Single-Site Catalysts. *Angew. Chem., Int. Ed.* **2005**, *44* (16), 2336−2354.

(7) Lang, S. M.; Bernhardt, T. M. Gas Phase Metal Cluster Model Systems for Heterogeneous Catalysis. *Phys. Chem. Chem. Phys.* **2012**, *14* (26), 9255−9269.

(8) Ding, X. L.; Wu, X. N.; Zhao, Y. X.; He, S. G. C−H Bond Activation by Oxygen-Centered Radicals over Atomic Clusters. *Acc. Chem. Res.* **2012**, *45* (3), 382−390.

(9) Wang, P. K.; Xie, H.; Guo, J. P.; Zhao, Z.; Kong, X. T.; Gao, W. B.; Chang, F.; He, T.; Wu, G. T.; Chen, M. S.; Jiang, L.; Chen, P. The Formation of Surface Lithium−Iron Ternary Hydride and its Function on Catalytic Ammonia Synthesis at Low Temperatures. *Angew. Chem., Int. Ed.* **2017**, *56* (30), 8716−8720.

(10) Schwarz, H. Metal-Mediated Activation of Carbon Dioxide in the Gas Phase: Mechanistic Insight Derived from a Combined Experimental/Computational Approach. *Coord. Chem. Rev.* **2017**, *334*, 112−123.

(11) Weber, J. M. The Interaction of Negative Charge with Carbon Dioxide − Insight into Solvation, Speciation and Reductive Activation from Cluster Studies. *Int. Rev. Phys. Chem.* **2014**, *33* (4), 489−519.

(12) Wang, G. J.; Zhou, M. F. Infrared Spectra, Structures and Bonding of Binuclear Transition Metal Carbonyl Cluster Ions. *Chin. J. Chem. Phys.* **2018**, *31* (1), 1−11.

(13) Yuan, Q. Q.; Zhang, J. M.; Zou, J. H.; Fan, H. J.; Jiang, L.; Xie, H. Photoelectron Velocity Map Imaging Spectroscopic and Theoretical Study of Heteronuclear Vanadium-Nickel Carbonyl Anions $VNi(CO)_n^-$ (n = 2−6). *J. Chem. Phys.* **2018**, *149* (14), 144305.

(14) Xie, Y. M.; Schaefer, A.; King, R. B. Binuclear Homoleptic Iron Carbonyls: Incorporation of Formal Iron−Iron Single, Double, Triple, and Quadruple Bonds, $Fe_2(CO)_x$ (x = 9, 8, 7, 6). *J. Am. Chem. Soc.* **2000**, *122*, 8746−8761.

(15) Liu, Z. L.; Xie, H.; Zou, J. H.; Fan, H. J.; Tang, Z. C. Observation of Promoted C−O Bond Weakening on the Heterometallic Nickel−Silver: Photoelectron Velocity-Map Imaging Spectroscopy of $AgNi(CO)_n^-$. *J. Chem. Phys.* **2017**, *146* (24), 244316.

(16) Zhang, J. M.; Li, Y.; Bai, Y.; Li, G.; Yang, D.; Zheng, H. J.; Zou, J. H.; Kong, X. T.; Fan, H. J.; Liu, Z. L.; Jiang, L.; Xie, H. CO Oxidation on the Heterodinuclear Tantalum−Nickel Monoxide Carbonyl Complex Anions. *Chem. Phys. Lett.* **2021**, *32* (2), 854−860.

(17) Zhang, J. M.; Li, Y.; Liu, Z. L.; Li, G.; Fan, H. J.; Jiang, L.; Xie, H. Ligand-Mediated Reactivity in CO Oxidation of Niobium−Nickel Monoxide Carbonyl Complexes: The Crucial Roles of the Multiple Adsorption of CO Molecules. *J. Phys. Chem. Lett.* **2019**, *10* (7), 1566−1573.

(18) Jiang, L.; Xu, Q. Observation of Anomalous C-O Bond Weakening on Discandium and Activation Process to CO Dissociation. *J. Am. Chem. Soc.* **2005**, *127* (1), 42−43.

(19) Meyer, F.; Chen, Y. M.; Armentrout, P. B. Sequential Bond Energies of $Cu(CO)_x^+$ and $Ag(CO)_x^+$ (x = 1−4). *J. Am. Chem. Soc.* **1995**, *117* (14), 4071−4081.

(20) Zhang, N.; Luo, M. B.; Chi, C. X.; Wang, G. J.; Cui, J. M.; Zhou, M. F. Infrared Photodissociation Spectroscopy of Mass-Selected Heteronuclear Iron−Copper Carbonyl Cluster Anions in the Gas Phase. *J. Phys. Chem. A* **2015**, *119* (18), 4142−4150.

(21) Li, G.; Zhang, J. M.; Xie, H.; Kong, X. T.; Jiang, L. Ligand-Enhanced CO Activation by the Early Lanthanide−Nickel Heterodimers: Photoelectron Velocity-Map Imaging Spectroscopy of $LnNi(CO)_n^-$ (Ln = La, Ce). *J. Phys. Chem. A* **2018**, *122* (15), 3811−3818.

(22) Ju, B. M.; Zhang, Z. H.; Kong, X. T.; Zou, J. H.; Li, G.; Xie, H.; Jiang, L. Photoelectron Velocity Map Imaging Spectroscopy of Group 14 Elements and Iron Tetracarbonyl Anionic Clusters $MFe(CO)_4^-$ (M = Si, Ge, Sn). *J. Chem. Phys.* **2024**, *160* (4), 044307.

(23) Jin, X. Y.; Wang, G. J.; Zhou, M. F. Mg(i)−Fe(−ii) and Mg(0)−Mg(i) Covalent Bonding in the $MgnFe(CO)_4^-$ (n = 1, 2) Anion Complexes: An Infrared Photodissociation Spectroscopic and

Theoretical Study. *Phys. Chem. Chem. Phys.* **2023**, *25* (11), 7697−7703.
(24) Wang, G. J.; Zhao, J.; Hu, H. S.; Li, J.; Zhou, M. F. Formation and Characterization of $BeFe(CO)_4^-$ Anion with Beryllium−Iron Bonding. *Angew. Chem., Int. Ed.* **2021**, *60* (17), 9334−9338.
(25) Chi, C. X.; Wang, J. Q.; Qu, H.; Li, W. L.; Meng, L. Y.; Luo, M. B.; Li, J.; Zhou, M. F. Preparation and Characterization of Uranium−Iron Triple-Bonded $UFe(CO)_3^-$ and $OUFe(CO)_3^-$ Complexes. *Angew. Chem., Int. Ed.* **2017**, *56* (24), 6932−6936.
(26) Wang, J. Q.; Chi, C. X.; Hu, H. S.; Meng, L. Y.; Luo, M. B.; Li, J.; Zhou, M. F. Triple Bonds Between Iron and Heavier Group 15 Elements in $AFe(CO)_3^-$ (A = As, Sb, Bi) Complexes. *Angew. Chem., Int. Ed.* **2018**, *57* (2), 542−546.
(27) Wang, J. Q.; Chi, C. X.; Lu, J. B.; Meng, L. Y.; Luo, M. B.; Hu, H. S.; Zhou, M. F.; Li, J. Triple Bonds between Iron and Heavier Group-14 Elements in the $AFe(CO)_3^-$ Complexes (A = Ge, Sn, and Pb). *Chem. Commun.* **2019**, *55* (40), 5685−5688.
(28) Wang, J. Q.; Chi, C. X.; Hu, H. S.; Li, X.; Luo, M. B.; Li, J.; Zhou, M. F. Multiple Bonding Between Group 3 Metals and $Fe(CO)_3^-$. *Angew. Chem., Int. Ed.* **2020**, *59* (6), 2344−2348.
(29) Zou, J. H.; Xie, H.; Yuan, Q. Q.; Zhang, J. M.; Dai, D. X.; Fan, H. J.; Tang, Z. C.; Jiang, L. Probing the Bonding of CO to Heteronuclear Group 4 Metal−Nickel Clusters by Photoelectron Spectroscopy. *Phys. Chem. Chem. Phys.* **2017**, *19* (15), 9790−9797.
(30) Qu, H.; Kong, F. C.; Wang, G. J.; Zhou, M. F. Infrared Photodissociation Spectroscopy of Heterodinuclear Iron−Zinc and Cobalt−Zinc Carbonyl Cation Complexes. *J. Phys. Chem. A* **2017**, *121* (8), 1627−1632.
(31) Wang, G. J.; Chi, C. X.; Cui, J. M.; Xing, X. P.; Zhou, M. F. Infrared Photodissociation Spectroscopy of Mononuclear Iron Carbonyl Anions. *J. Phys. Chem. A* **2012**, *116* (10), 2484−2489.
(32) Wang, G. J.; Cui, J. M.; Chi, C. X.; Zhou, X. J.; Li, Z. H.; Xing, X. P.; Zhou, M. F. Bonding in Homoleptic Iron Carbonyl Cluster Cations: A Combined Infrared Photodissociation Spectroscopic and Theoretical Study. *Chem. Sci.* **2012**, *3* (11), 3272−3279.
(33) Benzi, P.; Operti, L.; Vaglio, G. A.; Volpe, P.; Speranza, M.; Gabrielli, R. Gas Phase Ion−Molecule Reactions of Monogermane with Carbon Oxides and Ethylene: Formation of Germanium-Carbon Bonds. *J. Organomet. Chem.* **1989**, *373* (3), 289−300.
(34) Sparnaay, M. J. The Donor and Acceptor Character of Surface States on Germanium as Affected by the Adsorption of Carbon Monoxide. *Surf. Sci.* **1969**, *13* (1), 99−109.
(35) Cheng, Y. T.; Wan, H. W.; Chu, T. Y.; Pi, T. W.; Kwo, J.; Hong, M. Scavenging Segregated Ge on Thin Single-Crystal Si Epitaxially Grown on Ge. *ACS Appl. Electron. Mater.* **2021**, *3* (10), 4484−4489.
(36) Jung, S. C.; Kim, H. J.; Kang, Y. J.; Han, Y. K. Advantages of Ge Anode for Na-Ion Batteries: Ge vs Si and Sn. *J. Alloys Compd.* **2016**, *688*, 158−163.
(37) Hudait, M. K.; Johnston, S. W.; Das, M. R.; Karthikeyan, S.; Sahu, P. P.; Das, J.; Zhao, J.; Bodnar, R. J.; Joshi, R. Carrier Recombination Dynamics of Surface-Passivated Epitaxial (100) Ge, (110) Ge, and (111) Ge Layers by Atomic Layer Deposited Al_2O_3. *ACS Appl. Electron. Mater.* **2023**, *5* (6), 3350−3361.
(38) Peng, B.; Gu, F. L.; Zhang, X. H.; Luo, Q.; Li, Q. S. Theoretical Study on Homoleptic Mononuclear and Binuclear Ruthenium Carbonyls $Ru(CO)_n$ (n= 3−5) and $Ru_2(CO)_n$ (n = 8, 9). *Sci. China, Ser. B: Chem.* **2009**, *52* (11), 1938−1944.
(39) Zhang, Z. F.; Su, M. D. The Mechanistic Investigations of Photochemical Decarbonylations and Oxidative Addition Reactions for $M(CO)_5$ (M = Fe, Ru, Os) Complexes. *RSC Adv.* **2019**, *9* (5), 2626−2640.
(40) Yang, J. D.; Wang, X.; Zhang, W. Q.; Zhang, G. F.; Gao, Z. W. Formation of a Robust Ru_4O_4 Skeleton with Two $Ru_2(CO)_4$ Units in Criss−Cross Configuration. *RSC Adv.* **2016**, *6* (37), 31196−31201.
(41) Yuan, Q.; Rohdenburg, M.; Cao, W.; Aprà, E.; Landmann, J.; Finze, M.; Warneke, J.; Wang, X. B. Isolated $[B_2(CN)_6]^{2-}$: Small Yet Exceptionally Stable Nonmetal Dianion. *Chem. Phys. Lett.* **2021**, *12* (50), 12005−12011.
(42) Tozer, D. J.; Handy, N. C. Improving virtual Kohn−Sham orbitals and eigenvalues: Application to excitation energies and static polarizabilities. *J. Chem. Phys.* **1998**, *109*, 10180−10189.

https://doi.org/10.1021/acs.jpclett.4c01532
J. Phys. Chem. Lett. 2024, 15, 6952−6957